Biochimica et Biophysica Acta 1848 (2015) 886–893

Contents lists available at ScienceDirect

Biochimica et Biophysica Acta

journal homepage: www.elsevier.com/locate/bbamem

Unraveling the impact of lipid domains on the dimerization processes of single-molecule EGFRs of live cells

Chien Y. Lin [a], Jung Y. Huang [b,*], Leu-Wei Lo [c]

[a] Department of Photonics, Chiao Tung University, Hsinchu 300, Taiwan, ROC
[b] The T.K.P. Research Center for Photonics, Chiao Tung University, Hsinchu 300, Taiwan, ROC
[c] Institute of Biomedical Engineering and Nanomedicine, National Health Research Institutes, Zhunan, Miaoli 350, Taiwan, ROC

ARTICLE INFO

Article history:
Received 25 August 2014
Received in revised form 21 November 2014
Accepted 18 December 2014
Available online 30 December 2014

Keywords:
Single-molecule
Receptor
Diffusion

ABSTRACT

Epidermal growth factor receptor (EGFR/ErbB1) is a transmembrane protein that can drive cell growth and survival via the ligand-induced dimerization of receptors. Because dimerization is a common mechanism for signal transduction, it is important to improve our understanding of how the dimerization process and membrane structure regulate signal transduction. In this study, we examined the effect of lipid nanodomains on the dimerization process of EGFR molecules. We discovered that after ligand binding, EGFR molecules may move into lipid nanodomains. The lipid nanodomains surrounding two liganded EGFRs can merge during their correlated motion. The transition rates between different diffusion states of liganded EGFR molecules are regulated by the lipid domains. Our method successfully captures both the sensitivity of single-molecule processes and statistic accuracy of data analysis, providing insight into the connection between the mobile clustering process of receptors and the hierarchical structure of plasma membrane.

1. Introduction

Live cells must execute a variety of cellular processes to survive in a changing environment. These cellular processes can be organized into three networks: the signaling network, transcription regulation network, and metabolic network [1–5]. The signaling network is responsible for relaying messages from the external environment to the cellular nucleus. The first event of signaling processes occurs at various types of receptors on the plasma membrane of a live cell. One such receptor is the epidermal growth factor receptor (EGFR/ErbB1), which drives cell growth and survival [6]. EGFR signaling is also responsible for several disease pathogeneses [7].

EGFR is a transmembrane protein containing an extracellular binding domain, a single transmembrane domain, and a cytoplasmic tyrosine kinase domain. Ligands such as epidermal growth factor (EGF) can bind to the extracellular domain and thus stimulate conformational changes in EGFR that promote receptor dimerization and the activation of the intracellular tyrosine kinase domain [6,8]. The phosphorylated tyrosine residues then act as docking sites for adaptor proteins, which further activate intracellular signaling cascades.

EGFR can form either a homodimer with an EGFR or heterodimers with other members of its receptor-family [8–10]. However, conclusions about the size of these molecular aggregates and the ligand-occupancy of the signaling complex remain controversial. Conventional steady-state ensemble approaches cannot be used to address the stochastic nature of receptors that encounter each other in the highly heterogeneous and fluidic plasma membrane. Recent advances in single-molecule fluorescent imaging and tracking have provided more insights into the behavior of intact EGFR on the plasma membranes of live cells [11–14]. Multiple EGFR signaling complexes have been found with varying degrees of stability. For example, by analyzing single-molecule trajectories the dissociative rate constants of dimers, $k_{off} = 1.24s^{-1}$, $k_{off} = 0.74s^{-1}$, and $k_{off} = 0.27s^{-1}$, have been determined for unoccupied, singly, and doubly liganded dimers, respectively [13]. It was found that dimers composed of two ligand-bound receptors are the most long-lived; their dissociative rate is more than four times slower than that of the unoccupied dimers. The association of EGF to monomer, unliganded dimers, and singly liganded dimers also differs. The doubly liganded dimers can enter into a very slow-moving state that correlates directly with receptor activation [13].

Recently, Lidke and his coworkers devised a two-color quantum-dot tracking method to visualize the state-dependent dimerization processes of human EGFR [13]. A three-state hidden Markov model was proposed to deduce the transition rates between free, co-confined, and dimerized states. They found that disruption of actin networks leads to the faster diffusion of receptor dimers and concluded that actin corrals establish the confinement zones for EGFRs. Sequestering cholesterol to disrupt lipid domains was found to have a minimal effect on the diffusion of EGFR dimers [13], suggesting that lipid domains have a negligible role in the confinement of EGFRs. However, as the native protein–lipid architectures and dynamics in the membrane environment are far

* Corresponding author.
E-mail address: jyhuang@faculty.nctu.edu.tw (J.Y. Huang).

http://dx.doi.org/10.1016/j.bbamem.2014.12.019
0005-2736/

from well understood, the existence and resulting functionality of a lipid nanoscale structure on EGFR dimerization remains controversial. In this study, we address the issue of the effect of lipid nanodomains on the dimerization process of EGFR molecules.

2. The energetic model

The plasma membranes of live cells are complex and highly heterogeneous [15–18]. Single-molecule tracking of a receptor protein can effectively probe into the microscopic environment and thermal fluctuations in a living cell. The influences of cellular objects or structures far separated from a receptor protein are negligible in the description of single-molecule diffusion of the protein. Thus, we can focus on the local environment of the protein. Based on our current knowledge of single-molecule diffusion in the plasma membrane, two types of interactions between a receptor protein and its local environment shall be taken into account. Firstly, the receptor protein can induce a local ordering of the surrounding lipid molecules via a lipid–protein interaction [19–21]. The receptor can also serve as a nucleation site to form a stable lipid domain and results in a free energy decrease. Secondly, there exist actin skeleton-induced membrane compartments [22,23]. Our model incorporates a cooperative action with the hierarchical structure of actin skeleton-induced membrane compartments, protein-induced lipid ordering domains and dynamic diffusion of receptor proteins. The basic ideas of the model are illustrated in Fig. 1(a) including the protein-induced lipid ordering and the actin skeleton-induced membrane compartment with length scales λ_x and λ_y.

The diffusion of a receptor protein in the plasma membrane can be described with the generalized Langevin equation [24]:

$$m\gamma\partial_t\vec{x_k} = -\nabla_k(\mathbb{V}+\mathbb{F}) + \overrightarrow{f_k} = -m\gamma\mathbb{U} + \overrightarrow{f_k}. \quad (1)$$

Here $\vec{x_k}$ is the position vector of the k-th receptor molecule and γ is the frictional parameter, which relates to the diffusion coefficient by $m\gamma = k_BT/D$. The fluctuation force $\overrightarrow{f_k}$ on the molecule fulfills the fluctuation-dissipation theorem $\left\langle \overrightarrow{f_k}(t)\overrightarrow{f_k}(t+\tau)\right\rangle = 2k_BTm\gamma\delta(\tau)$. We used a potential profile of $\mathbb{V} = \mathbb{V}_0 cos^n\left[\pi\left(\frac{x_k}{\lambda_x}+\frac{y_k}{\lambda_y}\right)\right]cos^n\left[\pi\left(\frac{x_k}{\lambda_x}-\frac{y_k}{\lambda_y}\right)\right]$ to model the interaction between the protein and actin corral with different gradients. By adjusting the exponent n and $\mathbb{V}_0$, we can control the interaction strength and range of the actin confinement in a membrane compartment.

We consider the lipid-dependent segregation of a mixture of raft and non-raft lipids as a lipid domain with an order parameter $\phi(r)$, which indicates the degree of enrichment of raft lipids. The enriched lipid rafts are $\phi(r) > 0$ (inside the red dashed circle in Fig. 1(a)) and the depleted raft lipids are $\phi(r) < 0$ (outside the red dashed circle in Fig. 1(a)). The dynamic evolution of the order parameter $\phi(r)$ follows the Cahn–Hilliard equation [25,26]

$$\partial_t\phi(r,t) = D\nabla^2\left[\partial_\phi\mathbb{F}\right] \quad (2)$$

with $\mathbb{F}$ denoting the Ginzburg–Landau functional of the lipid–lipid and protein–lipid interaction energy densities [27]. $\mathbb{F}$ can be expressed as

$$\mathbb{F} = \int\left[\frac{1}{2}\alpha\phi(r,t)^2 + \frac{1}{4}\beta\phi(r,t)^4 + \frac{1}{2}\chi|\nabla\phi(r,t)|^2 - \phi(r,t)S_P(r)\right]dA. \quad (3)$$

The Cahn–Hilliard equation is a coarse-grained version of Brownian-like diffusion [26]. According to the Landau mean field theory [25] of a physical system with an inversion symmetry $\phi(r) = \phi(-r)$, the first two terms of Eq. (3) describe the thermal stability of the system. The parameter α represents the binding energy of lipids (i.e., the energy needed to remove a lipid molecule from the lipid membrane), β denotes the interaction strength between lipid molecules, and the third term is

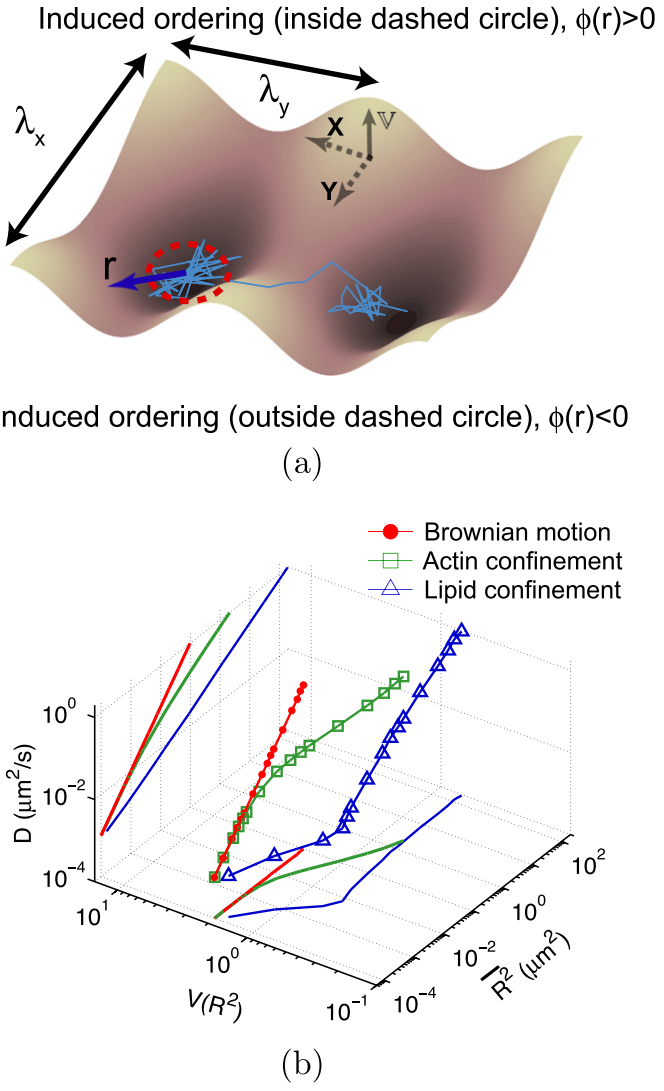

Fig. 1. Model and simulation result. (a) Schematic showing the model that involves the structure of actin skeleton-induced membrane compartments, protein-induced lipid ordering domains and dynamic diffusion of protein complexes. The actin skeleton is modeled with a potential barrier ($\mathbb{V}_0$) and the length scales (λ_x and λ_y). The region with induced lipid ordering (inside the red dashed circle) has $\phi(r) > 0$ for enriched raft lipids and outside has $\phi(r) < 0$ for depleted raft lipids. (b) Simulation results of $V(R^2)$ are plotted in the $V(R^2)) - R^2 - D$ space for single-molecule receptors under free Brownian motion (red solid circles), under confined diffusion by either actin corrals alone (green open squares, $\lambda_x = \lambda_y = 70nm$, barrier height $\mathbb{V}_0 = 0.5$ eV, and $n = 1$) or both actin corrals and lipid domains (blue open triangle). The initial condition of the lipid environment was assumed to be a homogeneous mixture with 40% raft lipids and 60% non-raft lipids ($\phi_0 = -0.2$). The length scales, confinement amplitude, and exponent of the actin corrals are $\lambda_x = \lambda_y = 70nm$, barrier height $\mathbb{V}_0 = 0.5$ eV, and $n = 3$.

from a line tension at the boundary of two different lipid phases. Typical values of the parameters are $\alpha = k_BT/2$, $\beta = k_BT/3$, and $\chi = 4k_BT\cdot\mu m^2$ for the plasma membrane system of live cells. The presence of a protein results in a force field that breaks the symmetry of lipid phases. The symmetry breaking yields a linear term with negative value in $\mathbb{F}$ [25]. Therefore, the lipid ordering $\phi(r) > 0$ induced by a protein ($S_P(r) = 1$) decreases the free energy of a lipid domain.

To evaluate the effect of the heterogeneities of plasma membrane on the movement of a receptor molecule, we solved Eqs. (1) and (2) self consistently to yield single-molecule trajectories and then calculated the variance $\sigma^2_{R^2}$ of the squared displacements $R^2(t)$. We present our simulation results in a plot of $V(R^2)$ versus $\overline{R^2(t)}$ with $V(R^2) = \sigma^2_{R^2}/$

$\left(\overline{R^2}\right)^2$ denoting the normalized variance of $R^2(t)$. An attractive feature of this data visualization scheme is that when a molecule repetitively visits (or stays long enough in) a membrane domain, the characteristic $\overline{R^2}$ and $V(R^2)$ of the domain will be imposed on the trajectory; this yields a peak feature at the corresponding position on the plot.

Fig. 1(b) shows the typical simulation results for the molecules under Brownian motion (red solid circles), and with the confinement from actin corrals alone (green open squares) or from both actin corrals and lipid domains (blue open triangles). For molecules under free diffusion (i.e., $\mathbb{U} = 0$) with the diffusion coefficient D in a lipid membrane varying from $10^{-4}\mu m^2/s$ to $10^{-1}\mu m^2/s$, $V(R^2)$ is kept at a constant of 2. With actin confinement only, for those slower species with $\overline{R^2(t)}$ less than the confined area, $V(R^2)$ remains close to 2. Only the fast species with $\overline{R^2(t)}$ larger than the confined area can experience the actin potential. That causes $V(R^2)$ to deviate from 2. For molecules moving under action of both actin corrals and lipid domains, the larger the lipid domain that the receptor molecules encounter, the larger the deviation of $V(R^2)$ from 2. This is due to the fact that the larger lipid domain yields a larger $\mathbb{U}$ and therefore a larger $\overline{R^2(t)}$ (see also Fig. S3 of SI). The smallest $V(R^2)$ is limited by the confinement effect from actin corrals. Detailed description of our theory and the simulation results will be published elsewhere [28].

3. Materials and methods

3.1. Cell culture and reagents

HeLa cells were cultured in Dulbecco's Modified Eagle's medium (DMEM) with 10 % (*v*/*v*) fetal bovine serum without phenol red. Before the single-molecule live-cell imaging, the cells were plated in a slide with eight-well chambers. After reaching 70–80% confluence, the cells were deprived of serum for 24 h. To label EGFR, the cells were incubated with 10 nM of anti-EGFR antibody (Thermo Scientific) for 15 min and washed three times with phosphate buffered saline (PBS). The cells were sequentially treated with IgG-Cy3 or IgG-Qdot-525 for 15 min and washed three times again with PBS. Biotin-EGF (Invitrogen) was conjugated to Alexa-488 or Qdot-585-streptavidin conjugate (Invitrogen) in PBS. To sequester the cholesterol molecules on the plasma membranes, 10 μg/mL nystatin was added to the cell culture for 1 h before staining with either the antibody or EGF.

3.2. Single-molecule optical measurement

Single-molecule fluorescence was measured with an inverted optical microscope (Olympus IX-71) equipped with a high numerical aperture (NA) oil immersion objective lens (APON 60XOTIRFM, NA 1.45, Olympus). The output from a blue (473 nm) solid-state laser was collimated and sent to the back focal plane of the objective lens to excite quantum dots in live cells. The same objective lens was used to collect the fluorescent signal from the sample. The fluorescent signals were filtered with a 473 nm Raman notch filter and then detected with an electron-multiplying charge coupled device (EMCCD, Cascade II 512 from Photometrics). The measurement procedure was controlled by a software program based on μ-manager. For fluorophore-labeled species, the trajectories were recorded with sampling rate 100 ms and duration 100 s. For Qdot-labeled species, the trajectories were recorded with sampling rate 25 ms and duration 100 s.

3.3. Data analysis

Coordinates of two-dimensional positions of single-molecule receptors were extracted from a set of fluorescent images. The nearest positions in consecutive frames were connected to form single-molecule trajectories using multiple-target tracing algorithm [31]. We extracted the events of confined diffusion from a single-molecule trajectory by using the confinement quantification procedure [32], which had been demonstrated to be highly reliable to distinguish the events of confined diffusion from hopping. After retrieving the confined diffusion events from single-molecule trajectories, the local square displacements were calculated for every three consecutive frames. A histogram of local square displacements and normalized variances $V(R^2)$ was presented as a 2D contour plot of $\overline{R^2}$ and $V(R^2)$.

3.4. Simulation

We discretized the generalized Langevin equation (Eq. (1)) and solved the discretized form with the Euler scheme. To simulate the lipid dynamics with the Cahn-Hilliard equation, we assumed that lipid diffusion is ten-times faster than protein. Thus, we used a time mesh of $\Delta t_l = 1$ ms and a spatial mesh $\Delta x_l = \Delta x_p = 50$nm to simulate the lipid dynamics. To correctly reflect the lipid–protein interaction ($\mathbb{F}$ of Eq. (3)), the local lipid environment was updated to every positional change of protein. The initial condition of the lipid environment was assumed to be a homogeneous mixture with 40% raft lipids and 60% non-raft lipids. In addition to the lipid–lipid and lipid–protein interactions described by $\mathbb{F}$, the driving force in the generalized Langevin equation involves an anchoring potential $\mathbb{V}$ from actin corral $\mathbb{V} = \mathbb{V}_0 cos^n \left[\pi\left(\frac{x_k}{\lambda_x} + \frac{y_k}{\lambda_y}\right)\right] cos^n \left[\pi\left(\frac{x_k}{\lambda_x} - \frac{y_k}{\lambda_y}\right)\right]$ with $\mathbb{V}_0$ denoting the confinement amplitude and λ_x and λ_y the length scale parameters. In the simulation $n = 1$ or 3, $\mathbb{V}_0 = 0.05$ eV, and $\lambda_x = \lambda_y = 70$ nm were used [22].

4. Results and discussions

4.1. Single-molecule tracking of EGFR in the plasma membrane of live cells

It remains a challenge to study cellular events in a live cell as living cells are highly heterogeneous and stochastically dynamic at the single-molecule level. To probe the diffusing EGFR molecules and their local cellular environment, we tagged EGFRs in the plasma membrane of living HeLa cells with cyanine 3 fluorophore (Ab-Cy3), as illustrated in Fig. 2. Fluorescent EGF, synthesized by conjugating EGF with Alexa 488 (EGF-Ax488), was used to activate the EGFRs. To investigate the dynamics of the dual-receptor complex, we can select a pair of liganded (EGF-Ax488-EGFR) and unliganded EGFR (Ab-Cy3-EGFR) or a pair of liganded EGFR complex (EGF-Ax488-EGFR) and studied their relative motions. We also employed the fluorescent resonant energy transfer (FRET) technique to reveal the dynamic dimerization structure of a

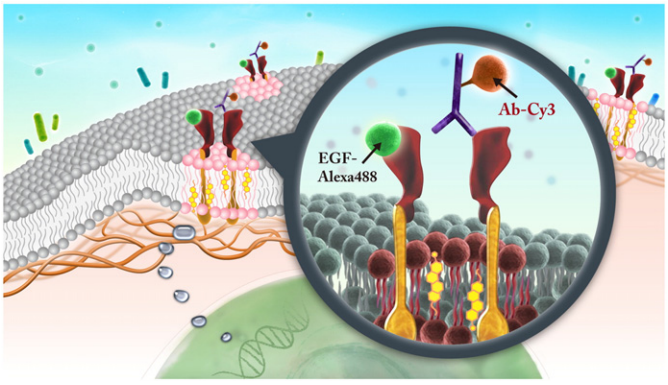

Fig. 2. Schematic diagram showing epidermal growth factor receptor (EGFR) dimers in the heterogeneous environment of plasma membrane. The meshwork underneath the lipid bilayer denotes the actin-based membrane skeleton. The labeling scheme used in this study: Ab-Cy3 denotes a cyanine 3 fluorophore conjugated to an EGFR antibody, and EGF-Ax488 is a fluorescent epidermal growth factor (EGF) synthesized by conjugating EGF with Alexa 488 fluorophore.

doubly liganded EGFR complex on live cells by activating the EGFR molecules with a mixture of EGF-Ax488 and EGF-Ax532 in equal molar ratio.

The same single-molecule tracking measurements were repeated after replacing the Cy3-tagged antibody (Ab-Cy3) with Ab-Qdot525, and the EFG-Ax488 with EGF-Qdot585. As quantum dots have brighter fluorescence and higher photostability than organic fluorophores, we increased the sampling rate to 25 ms and track durations of up to 100 s were achieved. We detected no difference between the two labeling schemes in the kinetics of EGFR on live cells. This comparison is important as the dimension of quantum dots is much larger than that of dye fluorophores and there are always concerns that different labeling schemes may cause alterations or dysfunction.

Typical single-molecule tracks of unliganded (Ab-Qdot525)-EGFR and liganded (EGF-Qdot585)-EGFR on the same live cells are shown in Fig. 3(a). Both the EGFR species exhibited confined diffusion in region 1 (marked by the red spots), interspaced by directed movement occurring in region 2. We bin the experimental mean-square displacements (MSD) in a histogram to deduce the probability density function (pdf) of the diffusion coefficient such that $P(D,\tau) = \left\langle \delta\left[D - \frac{R_\tau^2(t)}{4\tau}\right]\right\rangle$. Here $R_\tau^2(t) = \left\{\left[\vec{r}(t+\tau) - \vec{r}(t)\right]^2 + \left[(\vec{r}(t) - \vec{r}(t-\tau)\right]^2\right\}/2$ is the local MSD and $\langle \ldots \rangle$ denotes temporal sampling over all of the tracks in an ensemble. Fig. 3(b) shows the deduced data taken at a frame rate of $\tau = 25$ ms. For unliganded EGFR at rest, two sets of diffusers were revealed. The diffusion coefficient of the fast species peaked at 9 $\mu m^2/s$ and the slower one at 0.3 $\mu m^2/s$. EGF activation suppressed the population of 0.3 $\mu m^2/s < D < 6$ $\mu m^2/s$, whereas it increased the populations of $D \leq 0.1$ $\mu m^2/s$ and $D = 9$ $\mu m^2/s$. The quantum dot labeled samples, measured at a frame rate of $\tau = 100$ ms, yielded a slightly shifted $P(D,\tau)$ with the fast and the slower species peaking at 3 $\mu m^2/s$ and 0.12 $\mu m^2/s$, respectively. The shift to slower diffusion can be understood by considering that an anchoring effect or hindrance occurring on a much shorter temporal or spatial scale would be averaged out, resulting in a smaller diffusion coefficient. The down shifted $P(D,\tau)$ was also similar to that of the tracks of dye-labeled EGFR for the same frame rate. We also checked the concentration of the down-stream signaling complex (such as phosphorylated ERK) in the HeLa cells induced by the labeled EGFR and EGF and found it to be similar to that of the native EGFR and EGF, within our measurement accuracy (see Fig. S5 of SI).

4.2. Ligand binding can relocate EGFR to cholesterol-enriched lipid domains

We applied the above technique to analyze the experimental single-molecule tracks of unliganded Qdot525-Ab-EGFR of live HeLa cells at rest. The localization accuracy of our single-molecule optical apparatus was about 40 nm, implying an accuracy of 0.002 μm^2 for $\overline{R^2(t)}$ determination. Among the three peaks, labeled 1, 2, and 3 in Fig. 4(a), peak 2 was the most highly populated and had the most stable state given that the forward rate constant was $k_f(2 \rightarrow 3) = 3.7\ s^{-1}$, which was lower than that of the other forward kinetic process $k_f(1 \rightarrow 3) = 10.2\ s^{-1}$ and the backward rate constants $k_b(3 \rightarrow 1) = 32.4\ s^{-1}$ and $k_b(3 \rightarrow 2) = 39.3\ s^{-1}$. The three peaks were located at the $\left(\overline{R^2}, V\left(R^2\right)\right)$ coordinates of (0.01, 1.45), (0.02, 1.39), and (0.04, 1.33), respectively. The simulated curves shown in Fig. 1(b) for molecules under free Brownian motion (red dash line), under the confinement of actin corrals alone (green dash line) or both the actin corrals and lipid domains (blue dash curves), were replotted in Fig. 4 for comparison. The peak positions of the three states fell on the curve of the actin confinement, indicating that these unliganded receptor molecules were not free diffusers, but instead confined by actin corrals.

Lipid rafts are rich in saturated lipids and cholesterol [16,24]. We used nystatin to sequester the membrane cholesterol and disrupt the lipid raft domains in live cells. With the EGFR at rest as the control (see Fig. 4(a)), we examined the diffusion kinetics of liganded Qdot585-EGF-EGFR. Fig. 4(b) and (c) shows the $V\left(R^2\right) - \overline{R^2}$ plot of the liganded EGFR on activated native cells and nystatin-pretreated cells. In Fig. 4(b), three peaks were found to locate at (0.01, 0.42), (0.02, 0.47), and (0.04, 0.54) with associated forward transition rate constants of $k_f(1 \rightarrow 3) = 4.8\ s^{-1}$ and $k_f(2 \rightarrow 3) = 5.1\ s^{-1}$. These three peak positions agreed better with the model that includes the confinement effects of both actin corrals and lipid raft domains. Pretreating the cells with nystatin reduced the forward rate constants to $k_f(1 \rightarrow 3) = 3.4\ s^{-1}$ and $k_f(2 \rightarrow 3) = 3.6\ s^{-1}$, which were similar to those of the unliganded EGFR at rest. Furthermore, the three peaks of Fig. 4(c), found at (0.01, 1.39), (0.02, 1.33), and (0.04, 1.28), fell again on the curve of the actin confinement model, perhaps because unliganded EGFRs at rest are located outside the cholesterol-enriched lipid domains. EGF binding may cause the receptors to move into the cholesterol-enriched lipid domains, but pretreatment of cells with nystatin sequestered the membrane cholesterol and disrupted the lipid raft domains. This leads to local environmental changes in the ligand bound EGFR and reduced the rate constants of the diffusion kinetics. This interpretation is further supported by our observation that nystatin pretreatment did not alter the peak positions of unliganded EGFR on EGF-activated cells (see Fig. S1 of SI).

4.3. Duration of correlated motion of dual EGFR molecules

When a receptor molecule moves past a nearby receptor molecule, it may experience an interaction force that then induces a correlated

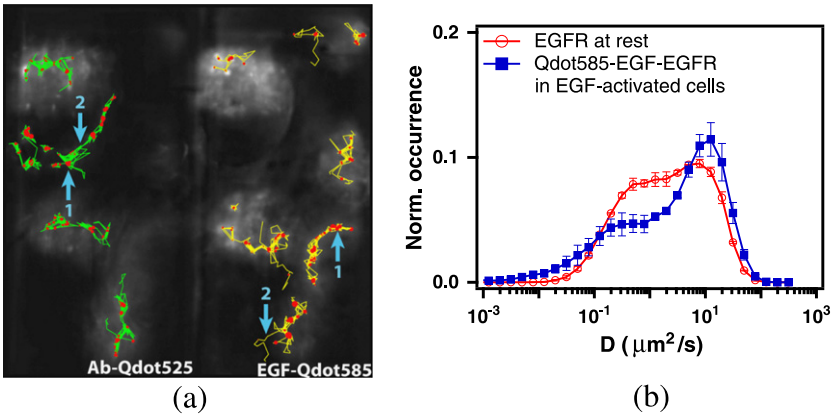

Fig. 3. Diffusive motions of EGFRs on live cells. (a) Single-molecule tracks of unliganded (Ab-Qdot525)-EGFR (green) and liganded (EGF-Qdot585)EGFR (yellow) superimposed on a dark field image of the live HeLa cells. The regions of confined diffusion are marked by the red spots. (b) Histogram of the diffusion coefficient of unliganded EGFR (red open circles) in the cells at rest and the liganded EGFR (blue solid squares) in EGF-activated cells.

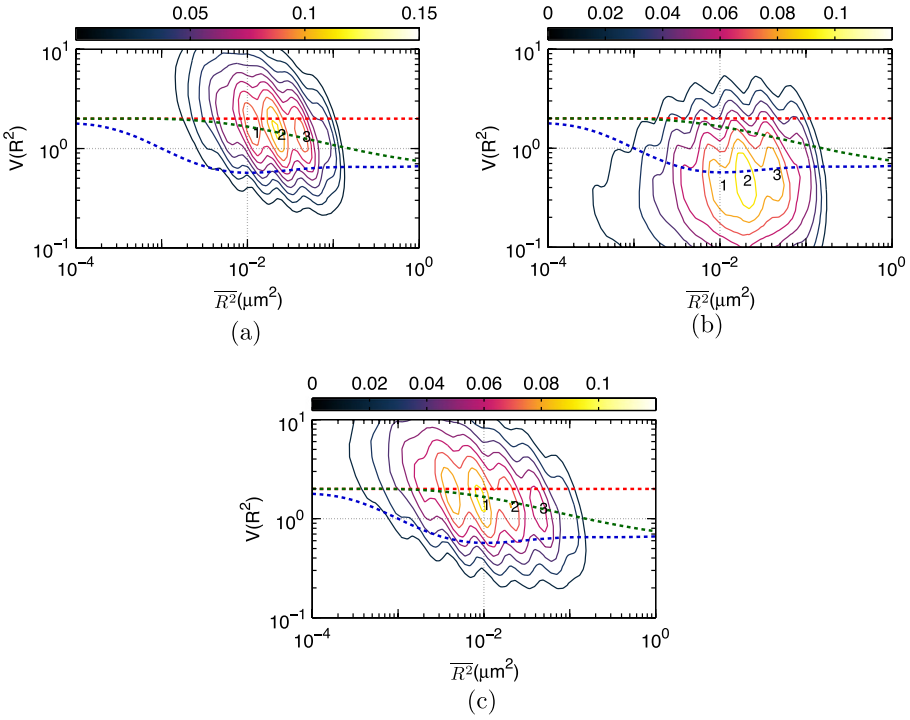

Fig. 4. (a) The plot of $V\left(R^2\right)-\overline{R^2}$ for unliganded Qdot525-Ab-EGFR on live HeLa cells at rest. Simulated curves of the peak positions for receptor molecules under free Brownian motion (red dash line), diffusive motion with the confinement from actin corrals alone (green dash line), or both the actin corrals and lipid raft domains (blue dash line) are included for comparison. The same plot is shown for liganded Qdot585-EGF-EGFR in (b) EGF-activated cells, and (c) activated cells pretreated with nystatin.

motion between the two receptor molecules. To analyze the correlated motion, we defined a parameter to more quantitatively reflect the degree of correlation:

$$\rho=\rho_r\times\rho_\phi=\frac{\sum_k\left(r_1(t_k)-\bar{r}_1\right)\left(r_2(t_k)-\bar{r}_2\right)}{\sqrt{\sum_k\left(r_1(t_k)-\bar{r}_1\right)^2}\sqrt{\sum_k\left(r_2(t_k)-\bar{r}_2\right)^2}}\frac{\sum_k\left(\phi_1(t_k)-\bar{\phi}_1\right)\left(\phi_2(t_k)-\bar{\phi}_2\right)}{\sqrt{\sum_k\left(\phi_1(t_k)-\bar{\phi}_1\right)^2}\sqrt{\sum_k\left(\phi_2(t_k)-\bar{\phi}_2\right)^2}}, \tag{4}$$

where r_i is the magnitude of a displacement by molecule i, and ϕ_i is the corresponding angle of the displacement. The summations were taken over a time mesh along the single-molecule tracks. Fig. 5(a) presents the histogram of the correlation in single-molecule tracks of paired Cy3-Ab-EGFR and Ax488-EGF-EGFR. As shown, the correlated portion of the tracks exhibited a broad distribution peaking at 0.5. The histogram of correlation for dual liganded EGFR protein pairs was similar to that shown in Fig. 5(a). We can reproduce the histogram by simulating the correlated motion of two Brownian-like particles with their spatial separation perturbed by a thermal fluctuation force. The simulated distribution of correlation peaks at $\rho = 0.5$.

By using the method, we were able to select the highly correlated segments from the single-molecule tracks and to analyze the duration of correlated motion. We set both ρ_r and ρ_ϕ to be larger than 0.9 to achieve a degree of correlation higher than 0.8. The results of correlation duration are presented in Fig. 5(b). The student's t-test ruled out the null assumption, but supported the distribution of correlation duration to comprise two groups with a significant level greater than 99%. Thus, we can conclude that prior to the formation of a dimer, the two EGFRs moved together for about 2 s and then departed from each other; a fraction of the EGFR pairs can move correlatively for a longer period and form a dimer. The long correlation duration could last as long as 10–30 s.

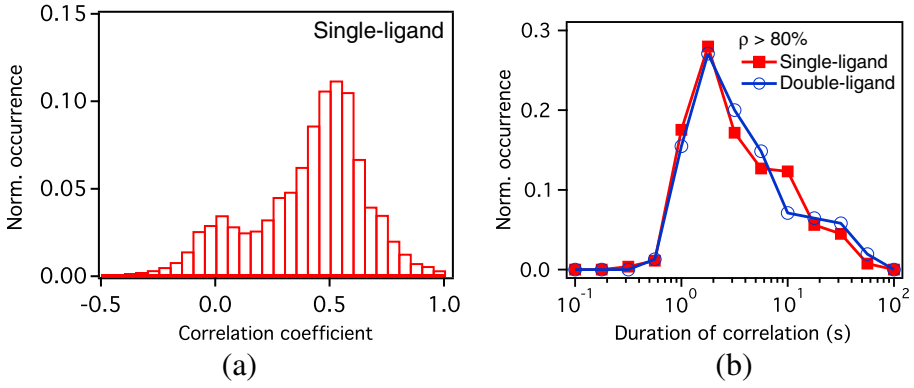

Fig. 5. Correlated motion of dual EGFRs on live cells. (a) Histogram of the degree of correlation existing in relative motion of unliganded Cy3-Ab-EGFR and liganded Ax488-EGF-EGFR. (b) Duration of correlated motion between the singly liganded EGFR pairs (red filled squares), and dually liganded EGFR pairs (blue open circles).

4.4. Correlated motions of dual EGFR molecules suggesting the liganded and unliganded species to reside in different lipid environments

As the receptors approached each other, their relative motion yielded insights into their interactions and the constraints imposed by membrane architecture. To unravel this important information, we plotted the $V\left(R^2\right)-\overline{R^2}$ of the correlated motion of unliganded Cy3-Ab-EGFR with liganded Ax488-EGF-EGFR. For comparison, the result of the unliganded EGFR molecules at rest is presented in Fig. 6(a), showing that EGFRs diffuse rapidly with the highest $V(R^2)$ approaching 2. As an unliganded Cy3-Ab-EGFR moved correlatively with a nearby liganded Ax488-EGF-EGFR, the diffusion motility $\overline{R^2}$ of state 1 decreased drastically to near 10^{-3}, accompanied by a reduction of $V(R^2)$ to 0.1 (Fig. 6(b)). It is interesting to note that the $V\left(R^2\right)-\overline{R^2}$ plot of the reverse case (Ax488-EGF-EGFR relative to Cy3-Ab-EGFR) differed in $\overline{R^2}$, as shown in Fig. 6(c). The resident time of Ax488-EGF-EGFR in state 2 also became longer and the $V(R^2)$ of both states 1 and 2 increased to 1, supporting the fact that the liganded Ax488-EGF-EGFR and unliganded Cy3-Ab-EGFR resided in different lipid environments.

The $V\left(R^2\right)-\overline{R^2}$ plot of the correlated motion between two liganded Ax488-EGF-EGFRs is presented in Fig. 7(a). Comparing the plot to that shown in Fig. 6(c), the $V(R^2)$ values of the two major states were found to decrease when the unliganded companion of Fig. 6(c) was replaced by liganded EGFR, perhaps because the lipid raft domains surrounding the two receptor molecules merge and yield a larger $\mathbb{U}$ (see Fig. S4 of SI) during the correlated motion. Pretreatment of the cells with nystatin (Fig. 7(b)) would disrupt the lipid nanodomains and decrease $V(R^2)$ further; owing to the stronger dimeric interaction experienced. This explanation is supported by our spatial separation data of the two liganded EGFRs in correlated motion presented in Fig. 7(c), showing that nystatin treatment shifted the distribution peak of the receptor separation from 150 nm to about 50 nm.

Thus, two liganded EGFRs in correlated motion can form a dimer. This can be further verified with two-color single-molecule FRET measurements of Ax488-EGF-EGFR and Ax532-EGF-EGFR. The histogram of FRET efficiency between the labeled receptors is presented in Fig. 7(d). The measured FRET efficiency on live cells (red open circles) peaked at 0.5 with a tail extending up to 0.8, indicating that the distance between two fluorophores on the bound ligands in EGFR dimers is heterogeneous, which can be attributed to the different orientations of fluorophores in varying domain sizes and lipid compositions. Pretreatment of the cells with nystatin rendered a FRET distribution to three groups, with a FRET efficiency centering at 0.3, 0.4, and 0.8, respectively. The highest FRET efficiency at 0.8 implies that without the constraint of lipid raft domains, the two fluorophores on liganded receptors in the dimers are allowed to close each other on nystatin-treated cells. However, the occurrence of FRET efficiency shall not be taken to represent the real population of dimer conformation because the highly nonlinear dependence of the FRET efficiency on distance at the two extreme ends.

As a final remark, we like to point out that our results also agree well with previous theoretical and experimental studies. For example, G. Orr et al. used single-molecule fluorescence imaging to track individual receptors and their dimerization partner and found that the diffusion pattern of both receptors can be altered by dwellings within lipid nanodomains [29]. They concluded that upon ligand stimulation the association of the receptors with lipid rafts is crucial to promote their rapid interactions [29]. Ligand stimulation of receptor proteins can increase the sizes and lifetimes of lipid raft domains [15]. To summarize the discoveries reported in the literature, A. Kusumi et al. proposed a cooperative action that involves the hierarchical structure of actin skeleton-induced membrane compartments, lipid raft domains and dynamic protein complexes [30].

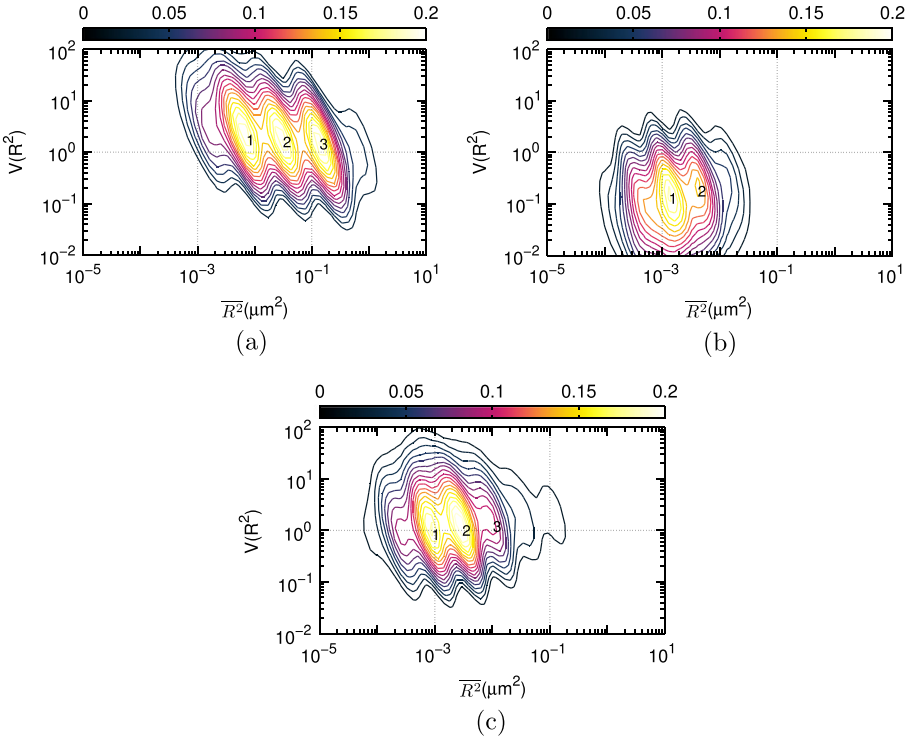

Fig. 6. $V\left(R^2\right)-\overline{R^2}$ plot of correlated motion of dual EGFRs with single ligand. (a) unliganded Cy3-Ab-EGFR on live HeLa cells at rest as the control, (b) unliganded Cy3-Ab-EGFR correlatively moving with a nearby liganded Ax488-EGF-EGFR companion, and (c) liganded Ax488-EGF-EGFR correlatively moving with a nearby unliganded Cy3-Ab-EGFR.

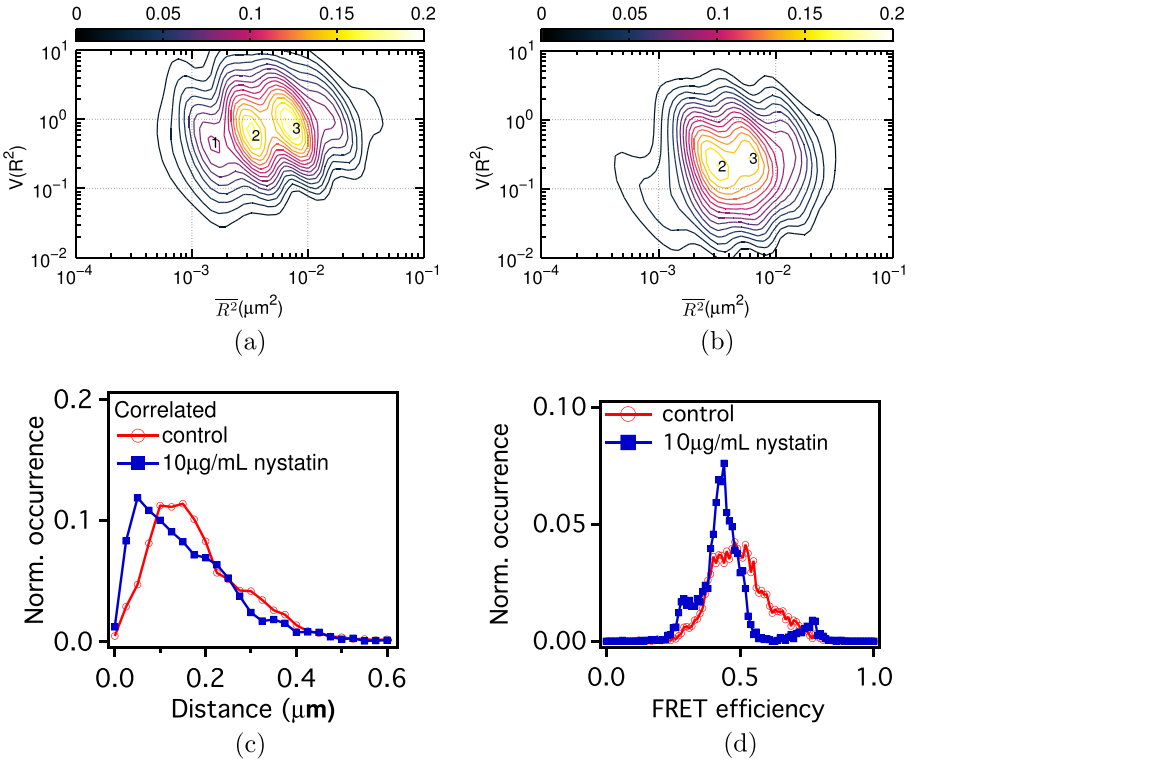

Fig. 7. $V\left(R^2\right)-\overline{R^2}$ plot of correlated motion of dual EGFRs with double ligands. (a) two liganded Ax488-EGF-EGFRs on live cells. (b) The same as (a) but on nystatin-pretreated cells. (c) Histogram of the relative distance between the two fluorophores on bound ligands in pairs of Ax488-EGF-EGFRs during their correlated motions. (d) Histogram of the FRET efficiency between Ax488-EGF-EGFR and Ax532-EGF-EGFR on stimulated live HeLa cells (red open circles: native, blue solid squares: pretreated with nystatin).

5. Conclusions

From the single-molecule trajectories of EGFRs on live cells, we discovered that after ligand binding, EGFR molecules may relocate to lipid raft domains, whereas unliganded species remain outside the cholesterol-enriched lipid domains. The transition rates between different diffusion states of liganded EGFR molecules are regulated by the lipid domains of live cells. The cholesterol-enriched lipid domains surrounding two liganded EGFRs can merge during their correlated motion. Our quantitative data analysis method captures dynamic receptor interactions at the single-molecule level, providing details that are often obscured in other methods. Because dimerization is a common mechanism for signal transduction, our approach can be applied to many other receptor systems to improve our understanding of how the dimerization process of receptors and membrane structure regulates signal transduction.

Acknowledgements

The authors thank the National Science Council Taiwan for its financial support under grant number NSC100-2112-M-009-015-MY3.

Appendix A. Supplementary data

Supplementary data to this article can be found online at http://dx.doi.org/10.1016/j.bbamem.2014.12.019.

References

[1] R. Sharan, S. Suthram, R.M. Kelley, T. Kuhn, S. McCuine, P. Uetz, T. Sittler, R.M. Karp, T. Ideker, Conserved patterns of protein interaction in multiple species, Proc. Natl. Acad. Sci. U. S. A. 102 (2004) 1974–1979.
[2] J.M. Vaquerizas, S.K. Kummerfeld, S.A. Teichmann, N.M. Luscombe, A census of human transcription factors: function, expression and evolution, Nat. Rev. Genet. 10 (2009) 252–263.
[3] N. Yosef, L. Ungar, E. Zalckvar, A. Kimchi, M. Kupiec, E. Ruppin, R. Sharan, Toward accurate reconstruction of functional protein networks, Mol. Syst. Biol. 5 (2009) 248.
[4] L. Hodgkinson, R.M. Karp, Optimization criteria and biological process enrichment in homologous multiprotein modules, Proc. Natl. Acad. Sci. U. S. A. 110 (2013) 10872–10877.
[5] J.E. Purvis, G. Lahav, Encoding and decoding cellular information through signaling dynamics, Cell 152 (2013) 945–956.
[6] A. Citri, Y. Yarden, EGFErbB signalling: towards the systems level, Nat. Rev. Mol. Cell Biol. 7 (2006) 505–516.
[7] C.L. Arteaga, J.A. Engelman, ErbB receptors: from oncogene discovery to basic science to mechanism-based cancer therapeutics, Cancer Cell 25 (2014) 282–303.
[8] M.A. Lemmon, J. Schlessinger, Cell signaling by receptor tyrosine kinases, Cell 25 (2010) 1117–1134.
[9] M.A. Lemmon, Ligand-induced ErbB receptor dimerization, Exp. Cell Res. 315 (2009) 638–648.
[10] Á. Szabó, J. Szöllősi, P. Nagy, Coclustering of ErbB1 and ErbB2 revealed by fret-sensitized acceptor bleaching, Biophys. J. 99 (2010) 105–114.
[11] Y. Teramura, J. Ichinose, H. Takagi, K. Nishida, T. Yanagida, Y. Sako, Single-molecule analysis of epidermal growth factor binding on the surface of living cells, EMBO J. 25 (2006) 4215–4222.
[12] I. Chung, R. Akita, R. Vandlen, D. Toomre, J. Schlessinger, I. Mellman, Spatial control of EGF receptor activation by reversible dimerization on living cells, Nature 464 (2010) 783–787.
[13] S.T. Low-Nam, K.A. Lidke, P.J. Cutler, R.C. Roovers, P.M.P. van Bergen en Henegouwen, B.S. Wilson, D.S. Lidke, ErbB1 dimerization is promoted by domain co-confinement and stabilized by ligand binding, Nat. Struct. Mol. Biol. 18 (2011) 1244–1249.
[14] M. Hiroshimaa, Y. Saekib, M. Okada-Hatakeyamab, Y. Sako, dynamically varying interactions between heregulin and ErbB proteins detected by single-molecule analysis in living cells, Proc. Natl. Acad. Sci. U. S. A. 109 (2012) 13984–13989.
[15] K. Simons, J.L. Sampaio, Membrane organization and lipid rafts, Cold Spring Harb. Perspect. Biol. 3 (2011) a004697.
[16] D. Lingwood, K. Simons, Lipid rafts as a membrane-organizing principle, Science 327 (2010) 46–50.
[17] H.A. Lucero, P.W. Robbins, Lipid rafts–protein association and the regulation of protein activity, Arch. Biochem. Biophys. 426 (2004) 205–224.
[18] A. Viola, N. Gupta, Tether and trap: regulation of membrane-raft dynamics by actin-binding proteins, Nat. Rev. Immunol. 7 (2007) 889–896.
[19] J. Dan, V. Nicolau, K. Burrage, R.G. Parton, J.F. Hancock, Identifying optimal lipid raft characteristics required to promote nanoscale protein–protein interactions on the plasma membrane, Mol. Cell. Biol. 26 (2006) 313–323.

[20] S. Türkcan, M.U. Richly, A. Alexandrou, J.-B. Masson, Probing membrane protein interactions with their lipid raft environment using single-molecule tracking and Bayesian inference analysis, PLoS ONE 8 (2013) e53073.
[21] D.L. Parton, A. Tek, M. Baaden, M.S.P. Sansom, Formation of raft-like assemblies within clusters of influenza hemagglutinin observed by MD simulations, PLoS Comput. Biol. 9 (2013) e1003034.
[22] K. Murase, T. Fujiwara, Y. Umemura, K. Suzuki, R. Iino, H. Yamashita, M. Saito, H. Murakoshi, K. Ritchie, A. Kusumi, Ultrafine membrane compartments for molecular diffusion as revealed by single molecule techniques, Biophys. J. 86 (2004) 4075–4093.
[23] A. Kusumi, C. Nakada, K. Ritchie, K. Murase, K. Suzuki, H. Murakoshi, R.S. Kasai, J. Kondo, T. Fujiwara, Paradigm shift of the plasma membrane concept from the two-dimensional continuum fluid to the partitioned fluid: high-speed single-molecule tracking of membrane molecules, Annu. Rev. Biophys. Biomol. Struct. 34 (2005) 351–378.
[24] D.M. Owen, A. Magenau, D. Williamson, K. Gaus, The lipid raft hypothesis revisited-new insights on raft composition and function from super-resolution fluorescence microscopy, BioEssays 34 (2012) 739–747.
[25] A. Bray, Theory of phase-ordering kinetics, Adv. Phys. 43 (1994) 357–459.
[26] T. Speck, J. Bialké, A.M. Menzel, H. Löwen, Effective Cahn–Hilliard equation for the phase separation of active Brownian particles, Phys. Rev. Lett. 112 (2014) 218304.
[27] J. Gomez-Llobregat, J. Buceta, R. Reigada, Interplay of cytoskeletal activity and lipid phase stability in dynamic protein recruitment and clustering, Sci. Rep. 3 (2013) 2608.
[28] C.Y. Lin, J.Y. Huang, L.W. Lo, Energetic modeling and single-molecule verification of dynamic regulation on receptor complexes by actin corrals and lipid raft domains, J. Chem. Phys. 141 (2014) 215102.
[29] G. Orr, D. Hu, S. Özçxelik, L.K. Opresko, H.S. Wiley, S.D. Colson, Cholesterol dictates the freedom of EGF receptors and HER2 in the plane of the membrane, Biophys. J. 89 (2005) 1362–1373.
[30] A. Kusumi, T.K. Fujiwara, N. Morone, K.J. Yoshida, R. Chadda, M. Xie, R.S. Kasai, K.G. Suzuki, Membrane mechanisms for signal transduction: the coupling of the meso-scale raft domains to membrane-skeleton-induced compartments and dynamic protein complexes, Semin. Cell Dev. Biol. 23 (2012) 126–144.
[31] A. Sergé, N. Bertaux, H. Rigneault, D. Marguet, Dynamic multiple-target tracing to probe spatiotemporal cartography of cell membranes, Nat. Methods 5 (2008) 687–694.
[32] N. Meilhac, L.L. Guyader, L. Salomé, N. Destainville, Detection of confinement and jumps in single-molecule membrane trajectories, Phys. Rev. E 73 (2006) 011915.